processes

MDPI

Article

Design of Downhole Robot Actuator System and Mechanical Behavior Analyses of the PRSM by Considering Elastic Errors and Radial Loads

Xuelian Dong, Haiyan Zhu, Qingyou Liu, Qiaozhu Wang * and Xingming Wang

State Key Laboratory of Oil and Gas Reservoir Geology and Exploitation, Chengdu University of Technology, Chengdu 610059, China; dongxuelian11@163.com (X.D.); zhuhaiyan040129@163.com (H.Z.); liuqy66@aliyun.com (Q.L.); upjzk@sina.com (X.W.)
* Correspondence: wangqiaozhu317103@163.com

Abstract: This paper designs a new class of actuators for the downhole traction robot system to achieve high-accuracy transmission, which is realized by the planetary roller screw mechanism (PRSM). As the downhole environment is a non-structure one, which increases the difficulty of the load analyses and distributions of the downhole robot system to complete a predesigned mission. Traditional achievements about the mechanical behavior analyses of PRSM ignore the effects of radial loads and torque elastic deformation errors, which are inevitable for the downhole robot actuator, and the results of which would affect the load distribution and fatigue life of the PRSM-aided actuator. To assist the complex task, in this study the mechanical behavior analyses of PRSM for the downhole robot system are investigated by considering axial loads, torque elastic deformation errors, and radial loads. Moreover, the calculation models for contact load distribution and fatigue life are established by utilizing the equivalent contact load and Hertz contact theory. Two cases for the robot actuator in the downhole environment are addressed, the results of which indicate that the contact load change and decrease with the thread growth direction of the PRSM, the first several threads bore most of the loads, and the last several threads only took a few loads. Additionally, the fatigue life reduces sharply under the condition that the axial loads, radial loads, and rotation speeds increase. Compared with the other two effectors, the fatigue life is more sensitive to the radial loads. The results show the sustainability of the presented screw–roller–nut and provide a potential reference for the downhole robot actuator motion analyses.

Keywords: downhole robot actuator; PRSM; elastic deformation errors; axial loads and radial loads; load distribution; fatigue life

check for updates

Citation: Dong, X.; Zhu, H.; Liu, Q.; Wang, Q.; Wang, X. Design of Downhole Robot Actuator System and Mechanical Behavior Analyses of the PRSM by Considering Elastic Errors and Radial Loads. *Processes* **2022**, *10*, 1520. https://doi.org/10.3390/pr10081520

Academic Editor: Raul D.S.G. Campilho

Received: 25 June 2022
Accepted: 27 July 2022
Published: 2 August 2022

1. Introduction

Horizontal wells are widely used in the exploration and development of deep sea complex oil and gas resources. As the depth and the length of horizontal wells continue to increase, it is urgent to create a new model to deal with the increasingly complex mission of resource explorations, which can be realized based on horizontal wells and downhole robot technologies.

The concept of the downhole robot was first proposed by H. Jørgen in 1987 [1], which can be divided into two categories according to its structural characteristics and application conditions: downhole traction robots and downhole drilling robots [2]. Downhole robots play an indispensable role in drilling and completion operations to transport downhole tools to designated locations, and to achieve explosive fracturing. Additionally, the downhole robot can solve the buckling deformation of coiled tubing, the difficulty of running downhole tubing strings in horizontal well logging, fracturing, and other operations. Nowadays, the downhole robot has been widely used in downhole operations in long horizontal complex wells.

The structure of the downhole robot mainly includes a right and left body-support mechanism, traction mechanism, power mechanism, and so on. As shown in Figure 1, according to their structures and different actuators, downhole traction robots can be divided into three categories, which are the wheeled traction robot, pedrail traction robot, and telescopic traction robot. Additionally, more concretely, the driving forces of the downhole robot can be founded as two kinds, i.e., hydraulic cylinder and motor. Compared with the other two traction robots, the telescopic type has a good performance in terms of passing over the obstacle. From the perspective of driving power in the hydraulic cylinder scheme, some complex oil circuits should be designed and arranged in a small robot system, which decreases the flexibility of the downhole robot system. On the other hand, the unnecessary oil circuit can be omitted in the motor driving framework, and the power supply and communication can be integrated. This motivates the motor-driven actuator design of this study.

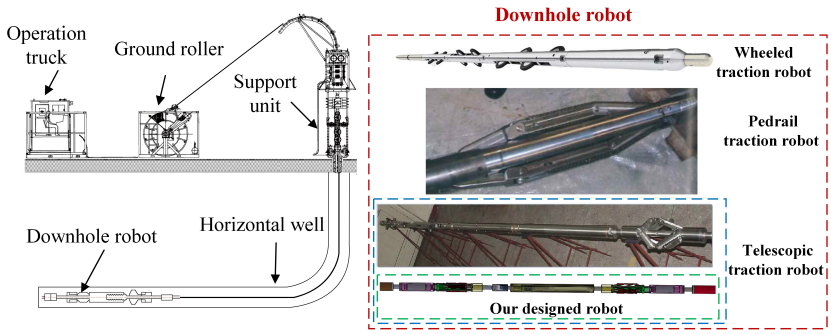

Figure 1. Brief introduction of the downhole robot system.

It should be noted that the traction devices used by the previous downhole robots are hydraulic telescopic and wheeled [3,4]. However, the wheeled downhole robots have a large diameter and cannot be used in tiny boreholes [5]. On the other hand, signal feedback is troublesome during the operation of the robots for the hydraulic power traction condition. Additionally, the solenoid valve is limited to withstand high temperatures; indeed, the solenoid valve and hydraulic oil passage are easy to enter and block impurities, which limits the application of the hydraulic telescopic power mechanism [6–8]. From the transmission accuracy and control response speed perspective, the planetary roller screw mechanism (PRSM) has been widely used in aerospace, ships, medical equipment, special machinery, weaponry, and other precision fields [9,10] owing to its high transmission accuracy in recent years. However, only a few studies have investigated the application of PRSM to downhole robot systems. This work presents a class of downhole robot systems, the traction actuator mechanism of which is a planetary roller screw traction mechanism one. The PRSM is a power unit that converts the rotational motion of the lead screw into the linear motion of the nut, which can achieve a precision transmission task. With the PRSM actuator mechanism, the actuator is driven by a motor rather than a hydraulic ram, which implies that the structure is simplified due to the omission of some hydraulic oil circuits. With the continuous development and application of long horizontal wells, the well structure will have local bending an inclination due to the change of deflection parameters in long-horizontal complex-structure wells. When the robot works in the downhole, the non-structural shaft wall will cause different degrees of extrusion to affect the robot. In addition, the high temperature and pressure in the downhole have also posed challenges to its mechanical behaviors and fatigue life.

There are many factors affecting the safety and stability of PRSM. The existing achievements could provide a theoretical basis for the load distribution calculation and fatigue life analysis. For example, in [11], the authors studied the effects of uniformly distributed loads on the carrying capacity of PRSM. Furthermore, an improved iterative algorithm was proposed for multi-objective optimization, such as for contact deformation and finding the

best pitch. In [12], Fu et al. studied the influences of unevenly distributed load on the transmission accuracy and life of PRSM; the results show that it will accelerate the destruction of the thread contact surface and reduce the transmission stability when the screw rotates at a high speed. The results in [13,14] studied the effects of assembly errors and external loads on PSRM, and safe transmission mechanisms were discussed. Aur′egan and Yao, et al., respectively, investigated the effects of wear behavior, uncertain factors of the elastic–plastic contact characteristics, and machining errors on the PRSM in [15,16]. In [17], the nature of the contact with friction between the threaded surfaces in a PRSM was investigated, and the calculation model was established and simulated. The achievements in [18,19] discussed the load sharing and pitch deviation of the PSRM. The results show that the deformation also has a great influence on the fatigue life. More recently, the transmission efficiency of PRSM was studied in [20–22]; for instance, Mamaev, et al. reached the conclusion that the stiffness and bearing capacity will increase the transmission efficiency of PSRM in [20]. Auregan, et al. in [21], verified that the reason for reducing the transmission efficiency of PSRM was the complete sliding of the PRSM pair, which was caused by the plastic–flow ratio between the thread engagements. In [22], the author discussed Hertz contact model and a multi-axial fatigue criterion of PSRM, and the results were applied to two cases to verify the reliability. However, the aforementioned results have rarely discussed the PRSM utilized in the downhole environment, which is more complex and has some new challenges. Furthermore, the coupled torque elastic deformations and radial loads for the PRSM of the downhole robot system not have been explored.

As aforementioned, the performance of PRSM were affected by multiple factors, including the external loads, elastic errors, and even the complex working conditions. In this note, a class of traction robot systems was designed. The PRSM is introduced as the actuator. Additionally, the mechanical behavior of the PRSM used in the downhole robot system was investigated. The load distribution and fatigue life calculation models are established. The contributions of this study can be highlighted as follows:

(1) A new actuator is designed for the downhole traction robot system. Compared with the aforementioned downhole robot in [6–8], in this note, the PRSM is introduced. Moreover, the driver power can be supported by a motor instead of the hydraulic cylinder, which indicates that some hydraulic oil circuits can be omitted and then the structure of the robot system can be simplified.
(2) The mechanical analyses of the PRSM in the downhole environment is investigated. This is different from the existing achievements in [18–20], where the load distributions are analyzed by considering axial loads and external deformations. For the downhole traction robot system, the working environment is a non-structure one, which means that the radial loads and torque deformations cannot be ignored, and the load distributions and fatigue life will be affected. In this note, we establish the calculation and fatigue life calculation models for the presented actuator by considering the axial loads, radial loads and torque elastic deformations, simultaneously, with the help of the equivalent contact load and Hertz contact theory.

The remainder of this study is organized as follows. In Section 2, the mechanical model is discussed and the problem is formulated. In Section 3, the elastic deformation error is analyzed. In Section 4, the mechanical behavior analysis is verified. In Section 5, some simulation results are given. Finally, we conclude this study in Section 6.

2. Mechanical Model and Problem Formulation

2.1. Downhole Robot System Actuator Model Analysis and Design

As mentioned before, two driving power mechanisms are contained in the telescope traction robots. In this subsection, the comparison results of the two driving power mechanisms in the telescopic traction robot is expressed in Table 1. Some more detail results of the downhole robots can be found in the work [1].

Table 1. Comparisons of two driving powers in downhole telescopic traction robot mode.

Power	Actuator	Model	Advantages and Analyses	Disadvantages
Hydraulic	Hydraulic cylinder	Telescopic traction robot	Accessories are necessary; less structure design freedom and the control of the cylinder is difficult	The sensor requirement is high and lacks of feedback data; control precision is not so high; signal transmission is difficult; control logic is complicated
Electro-hydraulic	Motor and hydraulic cylinder	Wheeled and Telescope	More structure flexibility, higher traction force; good performance of trade off velocity range	Difficult to control; larger size; requirement of sealing performance; more parameters to be adjusted
Motor (Our presented)	PRSM (Our presented)	Telescopic traction robot	Easy to control; more design freedom; integration of power supply and communication; sensor data can be transmitted	The mechanical behavior of the PRSM should be analyzed

In this study, we designed a new actuator for the telescopic traction robot to complete complex tasks in the downhole, as shown in Figure 2. The PRSM is introduced in the downhole robot system design scheme. In our presented robot, the power is supported by the motor, and the PRSM is driven by the motor. It should be mentioned that the PRSM in the robot system can help the robot walk forward in the downhole. However, as the downhole environment is complex, the PRSM will suffer from radial force and elastic deformation, which will affect the load distribution on the threads of the PRSM. To guarantee high transmission accuracy, the mechanical behavior analysis of the actuator in the downhole should be made.

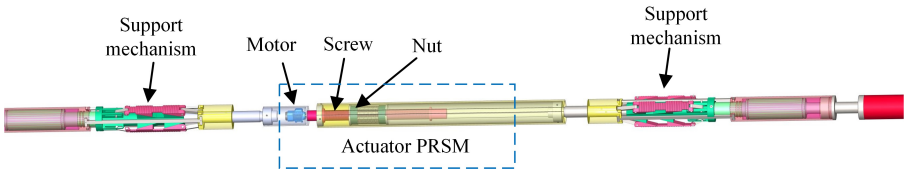

Figure 2. The presented downhole robot system

2.2. Analysis and Problem Formulation

The three dimensional model of the downhole robot system is shown in Figure 3a. The downhole robot system works in a retractable mode, as shown in Figure 3b, to complete the downhole task, eight steps are consisted in one cycle motion. The motion procedure of the robot system can be expressed as follows.

(a) Initial position. The left support cylinder, left support arm, PSRM, right support arm, and right support cylinder are all in the initial states, which are shown as in Figure 3;
(b) The left support mechanism of the robot system works with the cylinder;
(c) The motor rotates forward; the nut moves forward to drive the right support arm and the right main body to move forward;
(d) The left support arm contracts and moves forward with the left retractable cylinder;
(e) The right support arm completes the operation of the contract with the right support cylinder;
(f) The motor rotates in reverse and nut fixed; the screw draws the right support cylinder and the right main body to move forward;
(g) The right support arm completes the support operation with the right support cylinder;

(h) The left support arm completes the operation of the contract with the left support cylinder, and then goes back to state b;
Repeat steps b–h.

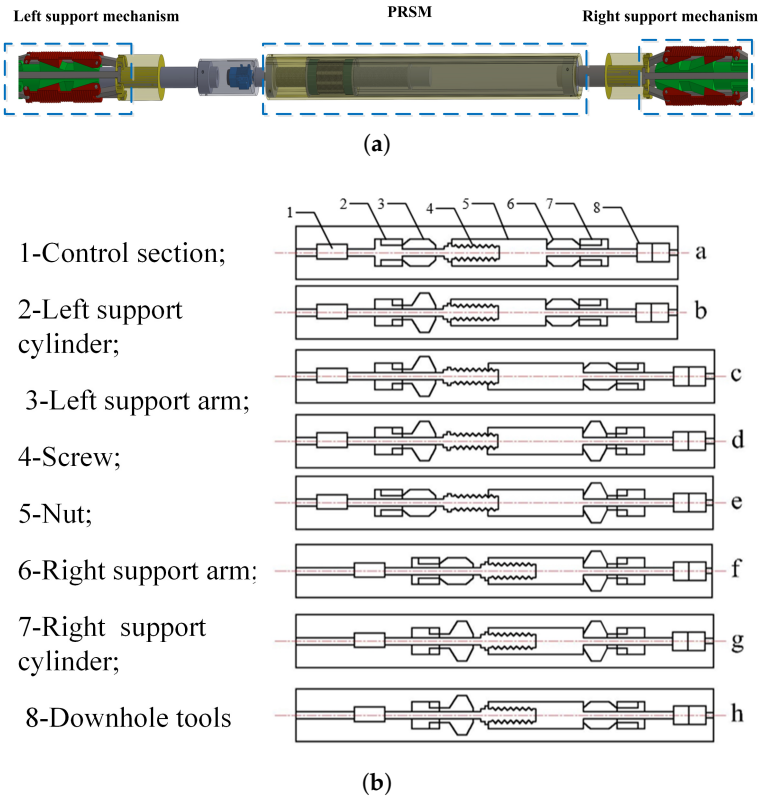

Figure 3. (**a**) The three-dimensional model of the downhole robot system; (**b**) the working mechanism of the downhole robot system.

It should be noted that during the working procedure, the mechanical behavior of PRSM is one of the most important parts of the robot system. In what follows, the contact load and the deformation of the PRSM are analyzed when the downhole robot works. The scheme of the PRSM of the robot system is depicted in Figure 4. We number the threads of each roller individually along with the axial direction. For the downhole robot system, two cases are contained to complete the predesigned task.

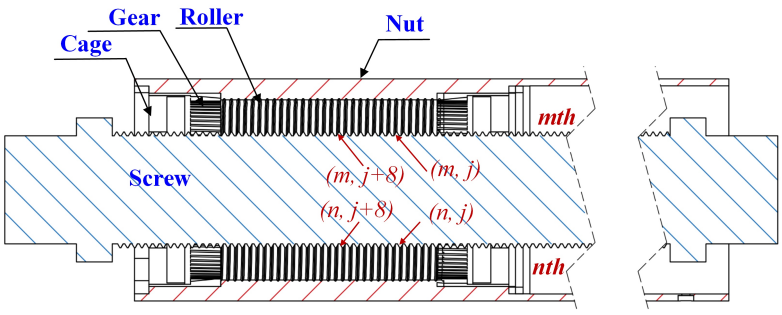

Figure 4. The threads number of each roller for the downhole robot system.

Case 1: The robot moves forward through the screw and roller, which are driven by the motor. In this condition, the nut is fixed and the screw is rotating and moving.

Case 2: The forward motion of the accessory support frame happens through the movement of the nut. In this condition, the screw is driven by the motor and only rotates without moving.

Before we give our main results, the following assumption is made.

Assumption 1 ([23]). *The deformations considered of the screw to roller and roller to the nut are elastic and satisfy the Hertz contact theory.*

Assumption 2. *The centrifugal force and gyroscopic moment are neglected.*

3. Elastic Deformation Error Analysis of the PRSM

3.1. Robot Elastic Deformation Error in Case 1

When the screw works in condition 1 in the downhole robot, it means that the motor drives the screw to rotate and move, and the axial load F_a is shown in Figure 5. In this condition, an additional radial load F_ζ exists as the screw drags some accessories and the downhole environment is non-structural. Additionally, a torsion deformation occurs when the screw works.

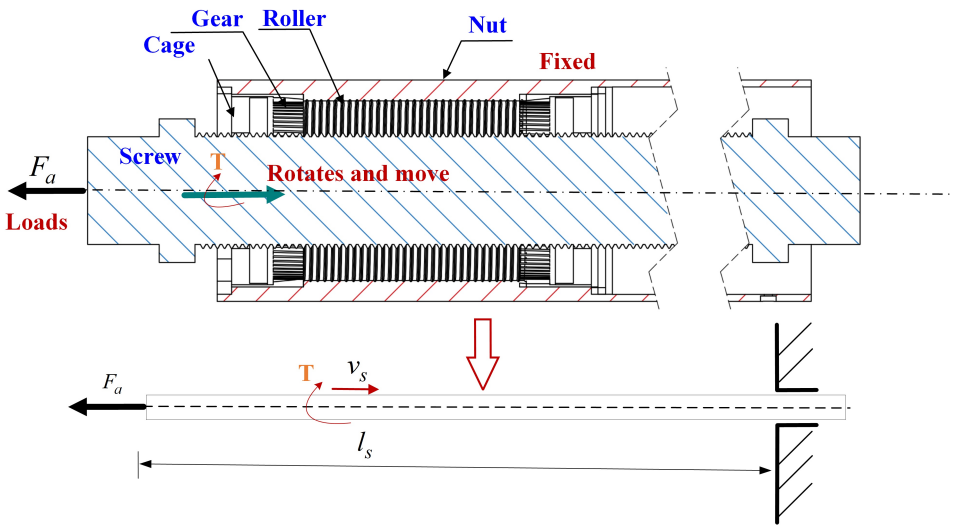

Figure 5. The diagram of the deformation in case 1.

For the downhole robot system in case 1, when the screw rotates and moves, the thread plays the main role in power and motion transmission. From the results in [24,25], the deformations caused by axial loads F_a and torsional T in the axis direction can be obtained as follows,

$$\lambda_{a1} = \frac{4F_a l_x}{E\pi d_z} \tag{1}$$

where λ_{a1} is the axial deformation caused by the tension load. l_x denotes the nut working position. E represents the elastic modulus of materials, and d_z is the diameter of screw thread.

$$\lambda_b = \frac{16Tl_s l_z}{\pi^2 d_z^4 G} \tag{2}$$

where λ_b represents the axial deformation caused by the driving torque. T is the driving torque. l_z denotes the lead of the screw. l_s is the length of screw against the torque, and G is the shear modulus.

In order to drag the accessories, the driving torque can be calculated as

$$T = \frac{F_a l_z}{2\pi\mu} \tag{3}$$

where μ denotes the transmission efficiency. From the Equation (3), Equation (2) can be reformulated as

$$\lambda_b = \frac{8F_a {l_z}^2 l_d}{\pi^3 d_z^4 G\mu} \tag{4}$$

Then, the total deformation error of the screw in the axial direction can be obtained as

$$\lambda_s = \lambda_{a1} + \lambda_b = \frac{4F_a l_x}{E\pi d_z} + \frac{8F_a {l_z}^2 l_d}{\pi^3 d_z^4 G\mu} \tag{5}$$

3.2. Robot Elastic Deformation Error in Case 2

As expressed in Figure 6, in this condition, only pressure deformation occurs in the nut, which means that the total deformation $\lambda_s = \lambda_{a2}$, and the deformation can be obtained as

$$\lambda_{a2} = \frac{4F_a l_x}{E\pi d_z} \tag{6}$$

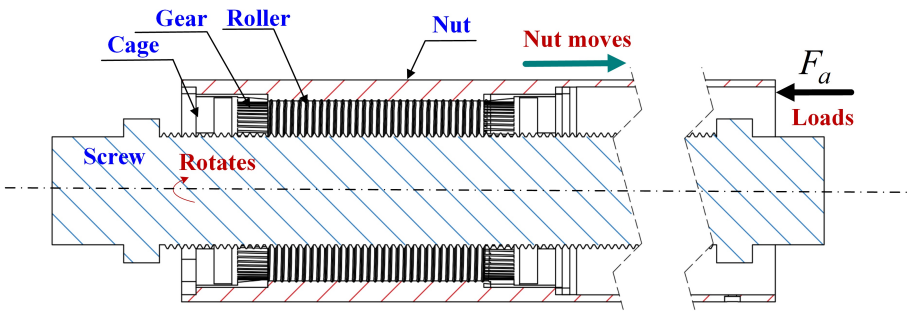

Figure 6. The diagram of the deformation in case 2.

Now we are in the position to analyze the contact deformation of the threads of screw-to-roller and roller-to-nut of the downhole robot system.

4. Mechanical Behavior Analysis

4.1. Robot Contact Deformation Analysis

As described in Figure 7, F_ζ denotes the radial loads. When the robot moves in the downhole, the PRSM is subjected to a non-structure radial force. As a result, a non-structure radial deformation of the roller at different position is generated correspondingly when the roller rotates. As expressed in Figure 7, the solid line denotes the initial position without the non-structure radial force, and the dashed line represents the new position when the nut is subjected to the radial loads. For the downhole robot system, the axial loads of screw and nut are the prior known knowledge and then the axial deformation can be obtained. It should be noted that the axial loads of each roller are not equal and difficult to calculate when the robot moves in the hole through the PRSM. In this study, the axial deformations of each roller of all threads are identical, and the radial deformations can be calculated by [26]

$$\zeta_{r(n,j)} = \zeta_r \cos\varphi_i \tag{7}$$

where ζ_r is the radial deformation, φ_i is the so-called position angle of the *ith* roller. By defining the angle between two adjacent rollers $\phi = \frac{2\pi n_a}{z}$, where z and n_a represent the number of rollers and work cycles. Then, φ_i can be calculated as

$$\varphi_i = \theta + (i-1)\phi \tag{8}$$

By changing the value of θ, the radial deformations of all the threads can be calculated.

In this study, the equivalent deformation concept is adopted, i.e., the normal deformations of the screw-to-roller and roller-to-nut are calculated by

$$\zeta_{e(n,j)} = \zeta_{a(n,j)} \sin\beta / \cos\varpi + \zeta_{r(n,j)} \cos\beta \cos\phi \tag{9}$$

where $\zeta_{e(n,j)}$ denotes the equivalent normal deformation of the thread, $\zeta_{a(n,j)}$ is the axial deformation, β and ϖ are the contact angle and helix angle, respectively.

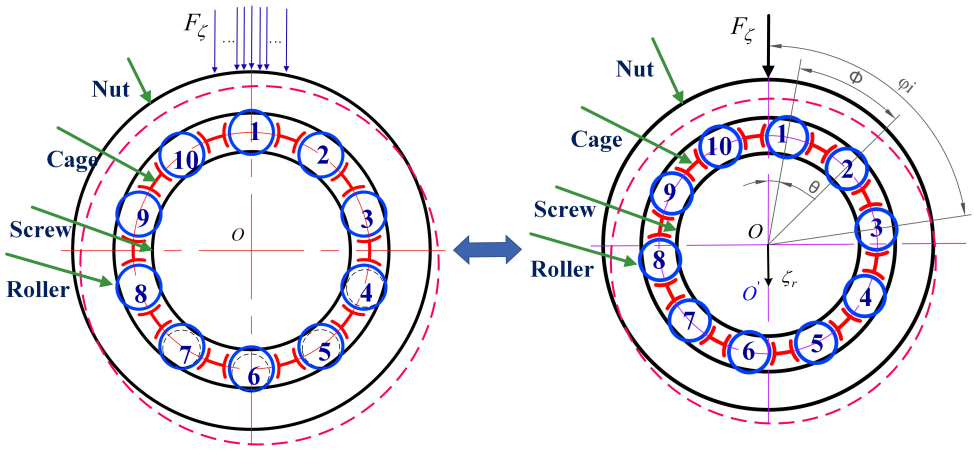

Figure 7. The diagram of deformation when subjected to radial loads.

From the Hertzian contact theory, the equivalent contact load of the contact point can be calculated via:

$$\Re_{e(n,j)} = \kappa\left(\frac{1}{\mathcal{G}_{ra}+\mathcal{G}_{rb}}\zeta_{e(n,j)}\right)^{\frac{3}{2}} \tag{10}$$

where κ is an indicator with $\kappa \in \{0,1\}$, which means that the threads are contacting when $\kappa = 1$, and the threads contact are abnormal when $\kappa = 0$. $\mathcal{G}_{ra}$ and $\mathcal{G}_{rb}$ represent the stiffness coefficients in the contact threads of the screw-to-roller and roller-to-nut, which can be obtained as [27]

$$\begin{cases} \mathcal{G}_{ra} = \frac{Q_{es}}{\pi m_{vs}}\sqrt[3]{9E^2\sum\rho_{as}/4} \\ \mathcal{G}_{rb} = \frac{Q_{en}}{\pi m_{vn}}\sqrt[3]{9E^2\sum\rho_{an}/4} \end{cases} \tag{11}$$

where Q_{es} and Q_{en} are two elliptic integral parameters of the screw-to-roller and roller-to-nut contact threads. m_{vs} and m_{vn} denote two semi-axis coefficients of the two contact threads. $\sum\rho_{as}$ and $\sum\rho_{an}$ represent the curvature sum of the two contact interfaces.

Remark 1. *In this study, the PRSM will be subjected to radial loads and axial loads during the working process in the downhole environment. However, in the existed achievements, most of the studies have only considered axial loads and the corresponding load distributions. There are rare results that have discussed the axial loads and radial loads simultaneously, and it should be noted that the loads of each roller of the PRSM are not equal when considering the radial loads. From this point of view, the equivalent contact load and Hertz contact theory are used to calculate the loads of all threads in this work.*

By combing Equations (7)–(11), the equilibrium equations in the radial and axial direction can be expressed by

$$\begin{cases} F_\zeta - \sum\limits_{n=1}^{N}\sum\limits_{j=1}^{P_z}\zeta_{e(n,j)}cos\beta\cos\phi = 0 \\ F_a - \sum\limits_{n=1}^{N}\sum\limits_{j=1}^{P_z}\zeta_{e(n,j)}\sin\beta\cos\varpi = 0 \end{cases} \tag{12}$$

where N and P_z stand for the numbers of rollers and threads. Furthermore, the axial load of the nth roller can be calculated by $F_{an} = \sum\limits_{j=1}^{P_z}\zeta_{e(n,j)}\sin\beta\cos\varpi$.

4.2. Robot Contact Load and Deformation Analysis

As described above, two cases are considered for the downhole robot system. In case 1, the screw is moving and the nut is fixed, which implies that the screw is in tension and

the nut is in compression $(S_c - N_t)$. In case 2, the screw rotates and the nut moves, which means that both the screw and nut are in compression $(S_c - N_c)$.

4.2.1. Deformation in $S_c - N_t$

As shown in Figure 8, denoting $\Im_{S(n,j)}$ and $\Im_{N(n,j)}$ as the thread contact loads of the screw and nut, when the PRSM works on the equilibrium point, the axial load for the case can be obtained as [23]

$$\Im_{S(n,j)} = \Im_{N(n,j)} = F_{an} - \sum_{h=1}^{j-1} \zeta_{e(n,h)} \sin\beta\cos\varpi \tag{13}$$

where $\zeta_{e(n,h)}$ can be solved by (12).

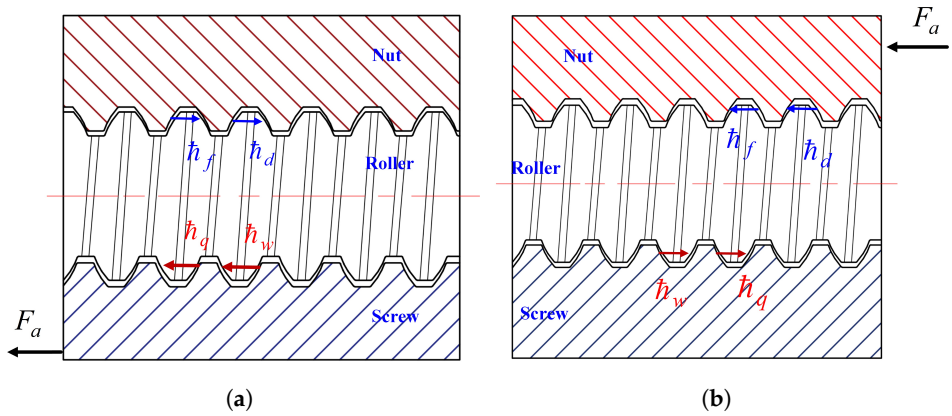

Figure 8. The sketches of the axial deformations in two cases.

Furthermore, when the screw is driven by a motor and subjected to external loads, some errors are evitable for the PRSM. Additionally, correspondingly, the following equations are derived

$$\hbar_{SZ(n,j)} = \hbar_w - \hbar_q = \frac{1}{\sin\beta\cos\varpi}\left(v_{SZ(n,j-1)} - v_{SZ(n,j)}\right) - \left(\Re_{SZ(n,j-1)} - \Re_{SZ(n,j)}\right) \tag{14}$$

where $\hbar_{SZ(n,j)}$ denotes the contact deformation in the screw to roller interface, which satisfies the Hertz condition. $v_{SZ(n,j-1)}$ and $v_{SZ(n,j)}$ represent two consecutive contact surfaces of the screw-to-roller. $\Re_{SZ(n,j-1)}$ and $\Re_{SZ(n,j)}$ are the contact interface axial elastic deformation errors of jth and $(j-1)th$ threads caused by driven torque and loads.

Similarly, the deformation occurs in the roller-to-nut with elastic errors can be calculated by

$$\hbar_{ZN(n,j)} = \hbar_d - \hbar_f = \frac{1}{\sin\beta\cos\varpi}\left(v_{ZN(n,j-1)} - v_{ZN(n,j)}\right) - \left(\Re_{ZN(n,j-1)} - \Re_{ZN(n,j)}\right) \tag{15}$$

where $v_{ZN(n,j-1)}$ and $v_{ZN(n,j)}$ express two consecutive contact surfaces deformations of roller to nut. $\Re_{ZN(n,j-1)}$ and $\Re_{ZN(n,j)}$ depict the elastic deformation errors of jth and $(j-1)th$ threads in the roller to nut interface caused by driven torque and loads.

From the Equations (14) and (15), the combined axial deformation errors by considering the elastic deformation errors can be obtained as

$$\begin{aligned}\hbar_{(n,j)} &= \hbar_w - \hbar_q + \hbar_d - \hbar_f \\ &= \tfrac{1}{\sin\beta\cos\varpi}\left(v_{SZ(n,j-1)} - v_{SZ(n,j)}\right) - \left(\Re_{SZ(n,j-1)} - \Re_{SZ(n,j)}\right) \\ &\quad + \tfrac{1}{\sin\beta\cos\varpi}\left(v_{ZN(n,j-1)} - v_{ZN(n,j)}\right) - \left(\Re_{ZN(n,j-1)} - \Re_{ZN(n,j)}\right) \\ &= \tfrac{1}{\sin\beta\cos\varpi}\left[v_{r(n,j-1)} - v_{r(n,j)}\right] - \left[\Re_{r(n,j-1)} - \Re_{r(n,j)}\right]\end{aligned} \tag{16}$$

where $v_{r(n,j-1)} = v_{SZ(n,j-1)} + v_{ZN(n,j-1)}$, $v_{r(n,j)} = v_{SZ(n,j)} + v_{ZN(n,j)}$, $\Re_{r(n,j-1)} = \Re_{SZ(n,j-1)} + \Re_{ZN(n,j-1)}$, $\Re_{r(n,j)} = \Re_{SZ(n,j)} + \Re_{ZN(n,j)}$.

For the downhole robot system in case 1, the axial deformation can also be formulated as

$$\begin{cases} \hbar_{S(n,j)} = \frac{\Im_{S(n,j)}\rho_a}{2E_sA_s} \\ \hbar_{N(n,j)} = \frac{\Im_{N(n,j)}\rho_a}{2E_NA_N} \end{cases} \tag{17}$$

where $\hbar_{S(n,j)}$ and $\hbar_{N(n,j)}$ represent the deformations in the screw-to-roller and roller-to-nut contact threads. ρ_a stands for the pitch, E_s. E_N , A_s, and A_N are the elastic modulus and cross sectional areas of the screw and nut, respectively. A_s and A_N can be calculated as $A_s = \pi {R_s}^2$, $A_N = \pi\left(R_{N1}^2 - R_{N2}^2\right)$, where R_s is the radius of the screw. R_{N1} and R_{N2} are the external and normal radius of nut.

In accordance with (17), similar to (16), the combined axial deformation can be obtained as

$$\hbar_{(n,j)} = \hbar_{S(n,j)} + \hbar_{N(n,j)} = \frac{\Im_{S(n,j)}\rho_a}{2E_sA_s} + \frac{\Im_{N(n,j)}\rho_a}{2E_NA_N} \tag{18}$$

By combing (16) and (18) yields,

$$\frac{\Im_{N(n,j)}\rho_a(A_N + A_s)\sin\beta\cos\varpi}{2E_sA_sA_N} = \left[v_{r(n,j-1)} - v_{r(n,j)}\right] - \sin\beta\cos\varpi\left[\Re_{r(n,j-1)} - \Re_{r(n,j)}\right] \tag{19}$$

According to the Hertzian contact theory, the following recursive condition can be derived

$$\begin{aligned} {\Re_{e(n,j-1)}}^{\frac{2}{3}} - {\Re_{e(n,j)}}^{\frac{2}{3}} = & \frac{\sin\beta\cos\varpi\left[\Re_{r(n,j-1)} - \Re_{r(n,j)}\right]}{(\mathcal{G}_{ra} + \mathcal{G}_{rb})} \\ & + \frac{\left(\sum_{j=1}^{P_z}\zeta_{e(n,j)}\sin\beta\cos\varpi - \sum_{h=1}^{j-1}\zeta_{e(n,h)}\sin\beta\cos\varpi\right)\rho_a(A_N + A_s)\sin\beta\cos\varpi}{2E_sA_sA_N(\mathcal{G}_{ra} + \mathcal{G}_{rb})} \end{aligned} \tag{20}$$

Now, we are in the position to analyze the deformation of case 2.

4.2.2. Deformation in $S_c - N_c$

For the $S_c - N_c$ condition, the axial load $\Im_{S(n,j)}$ and $\Im_{N(n,j)}$ of the screw and nut can be reorganized as [23]

$$\begin{cases} \Im_{N(n,j)} = F_{an} - \sum_{h=1}^{j-1}\zeta_{e(n,h)}\sin\beta\cos\varpi \\ \Im_{S(n,j)} = \sum_{h=1}^{j}\zeta_{e(n,h)}\sin\beta\cos\varpi \end{cases} \tag{21}$$

Moreover, accordingly, the deformations in the threads of the screw-to-roller and roller-to-nut in the axial direction can be calculated similarly as in Equations (14) and (15), while the roller-to-nut deformation is revised as

$$\hbar_{ZN(n,j)} = \hbar_f - \hbar_d = \frac{1}{\sin\beta\cos\varpi}\left(v_{ZN(n,j)} - v_{ZN(n,j-1)}\right) - \left(\Re_{ZN(n,j)} - \Re_{ZN(n,j-1)}\right) \tag{22}$$

From (14) and (22), the total axial deformation by considering the elastic deformation error can be obtained as

$$\begin{aligned} \hbar_{(n,j)} &= \hbar_w - \hbar_q + \hbar_f - \hbar_d \\ &= \tfrac{1}{\sin\beta\cos\varpi}\left(v_{SZ(n,j-1)} - v_{SZ(n,j)}\right) - \left(\Re_{SZ(n,j-1)} - \Re_{SZ(n,j)}\right) \\ &\quad + \tfrac{1}{\sin\beta\cos\varpi}\left(v_{ZN(n,j)} - v_{ZN(n,j-1)}\right) - \left(\Re_{ZN(n,j)} - \Re_{ZN(n,j-1)}\right) \\ &= \tfrac{1}{\sin\beta\cos\varpi}\left[\bar{v}_{r(n,j-1)} - \bar{v}_{r(n,j)}\right] - \left[\bar{\Re}_{r(n,j-1)} - \bar{\Re}_{r(n,j)}\right] \end{aligned} \tag{23}$$

where $\bar{v}_{r(n,j-1)} = v_{SZ(n,j-1)} + v_{ZN(n,j)}$, $\bar{v}_{r(n,j)} = v_{SZ(n,j)} + v_{ZN(n,j-1)}$, $\bar{\Re}_{r(n,j-1)} = \Re_{SZ(n,j-1)} + \Re_{ZN(n,j)}$, $\bar{\Re}_{r(n,j)} = \Re_{SZ(n,j)} + \Re_{ZN(n,j-1)}$.

By combing (17) and (21), it is straightforward that

$$\begin{aligned} \hbar_{(n,j)} = \hbar_{S(n,j)} + \hbar_{N(n,j)} &= \frac{\Im_{S(n,j)} A_N \rho_a}{2E_s A_s A_N} + \frac{\Im_{N(n,j)} A_s \rho_a}{2E_N A_s A_N} \\ &= \frac{\left(F_{an} - \sum_{h=1}^{j-1} \zeta_{e(n,h)} \sin\beta\cos\varpi\right) A_N \rho_a}{2E_s A_s A_N} + \frac{\sum_{h=1}^{j} \zeta_{e(n,h)} \sin\beta\cos\varpi \rho_a A_s \rho_a}{2E_N A_s A_N} \end{aligned} \tag{24}$$

Furthermore, according to the Hertzian contact theory, the corresponding recursive equation in case 2 can be obtained as

$$\begin{aligned} &\Re_{e(n,j-1)}{}^{\frac{2}{3}} - \Re_{e(n,j)}{}^{\frac{2}{3}} \\ &= \frac{\sin\beta\cos\varpi\left[\bar{\Re}_{r(n,j-1)} - \bar{\Re}_{r(n,j)}\right]}{\mathcal{G}_{ra} + \mathcal{G}_{rb}} + \frac{\sum_{h=1}^{j} \zeta_{e(n,h)} \sin\beta\cos\varpi \rho_a A_s \rho_a \sin\beta\cos\varpi}{2E_N A_s A_N (\mathcal{G}_{ra} + \mathcal{G}_{rb})} \\ &+ \frac{\left(F_{an}\sin\beta\cos\varpi - \sum_{h=1}^{j-1} \zeta_{e(n,h)} \sin^2\beta\cos^2\varpi\right) A_N \rho_a}{2E_s A_s A_N (\mathcal{G}_{ra} + \mathcal{G}_{rb})} \end{aligned} \tag{25}$$

In this subsection, the mechanical analyses of the presented PRSM have been made by referencing the work in [23] and some ball rollers in [26]. The calculation process seems similar to the results in [23]. For example, in Section 3.2, the recursive equations of the contact load on the threads of two cases have been calculated; for details see (20) and (25). In Sections 2.2.2 and 2.2.3 of the work in [23], the contact deformations are also calculated. The calculation ideas of the work in our study and [23] may be similar, and this can be explained as follows. On the one hand, the force analysis model after simplifying for the downhole traction robot actuator is similar to the work in [23], i.e., both the external loads are axial load and radial load, and the difference lies in that the driven torque elastic deformation is considered. Additionally, the parameters of the PRSM are designed according to the downhole traction robot working condition, which are different from the work in [23]. On the other hand, the contact theory used in the two achievements are similar. In our study and the work in [23], the equivalent Hertz contact theory is utilized to analyze the contact load distribution, which in return implies that some equations and calculation idea may similar.

4.3. Downhole Robot Contact Load and Deformation Coefficient Analysis

As depicted in the aforementioned part, for the downhole robot system, the driven torque and external loads will cause elastic deformations and even errors, which will degrade the transmission accuracy in return. It should be also noted that elastic deformations will cause the change of load distribution. By considering the elastic deformation, the deformation coefficient is investigated in this note. Similar to [23], to express the deformation rate, we define this coefficient as the ratio of the normal contact deformation in the condition without and with the elastic deformation errors.

$$\lambda_{(n,j)} = \frac{\zeta_{sw(n,j)}}{\zeta_{st(n,j)}} \tag{26}$$

where $\zeta_{sw(n,j)}$ and $\zeta_{st(n,j)}$ denote the normal contact deformation in the condition without and with the elastic deformation errors.

Here, by considering the contact load and the Hertzian contact theory, we have

$$\lambda_{(n,j)} = \left(\frac{\Re_{sw(n,j)}}{\Re_{st(n,j)}}\right)^{\frac{2}{3}} \tag{27}$$

where $\Re_{st(n,j)}$ and $\Re_{sw(n,j)}$, respectively, represent the contact loads by considering the elastic deformation errors or not.

When the PRSM works, the load distribution is very important. We introduce the load coefficient to better show the mechanical behavior of the PRSM, which is defined as follows

$$\varepsilon_{(n,j)} = \frac{\Re_{sw(n,j)}}{\min\left(\Re_{sw(n,j)}\right)} \tag{28}$$

where $\varepsilon_{(n,j)}$ is the load coefficient, $\Re_{sw(n,j)}$ denotes the minimum value of contact load $\min\left(\Re_{sw(n,j)}\right)$.

4.4. Fatigue Life Analysis

For the downhole robot system, the non-structured environment increases the difficulty of analysis of the PRSM. As the PRSM would work for a long time in the downhole, the PRSM switches back and forth between the two cases to guarantee the complex task. Moreover, the fatigue life is a crucial performance that should be emphasized. From the stress life method, the estimation of fatigue lifetime is given as follows [23,26]

$$L_S = \frac{N_s(\kappa_s + 1)}{60 w_s \kappa_s (\kappa_s + 2)} \tag{29}$$

where $N_s = {k_\alpha}^{m_s} N_0$, $\kappa_s = \frac{d_s}{d_r}$, w_s is the rotating speed. k_α and N_0 are the stress ratio and circulation of the material, m_s is an index corresponding to the material, and d_s and d_r are the diameters of the screw and roller, respectively.

Remark 2. *It should be noted that the effects of the fatigue of roller screws can be listed as materials, stress, working conditions, and other effectors, such as lubrication. Here, we use the fatigue life equation of ball screws to estimate the fatigue life of roller screws, which means that (29) is not an accurate result, it is an estimation of fatigue life.*

Remark 3. *In Section 2.4 of the work in [23], the authors have considered the lifetime and mechanical analyses for the PRSM when subjected to axial load, radial load, and machine errors. However, in this study, the considered PRSM is utilized in the downhole environment, the parameters and working conditions are different from the case in [23] but somewhat similar. We established our estimation lifetime model by referencing [23,26], and the ball rollers. The idea of the lifetime estimation model is similar to [23], and we hope we can consider some more complex conditions for the downhole robot actuator, such as the lubrication analysis and thermal analysis in our future work, and that we can establish some more accurate calculation model for the lifetime by carrying out some experimentation.*

5. Analytical Calculations and Discussions

In this section, some numerical analyses are given to show the validity of the presented model for the downhole robot system. The calculation flow can be seen in Figure 9, and the detail analysis parameters are given in Table 2.

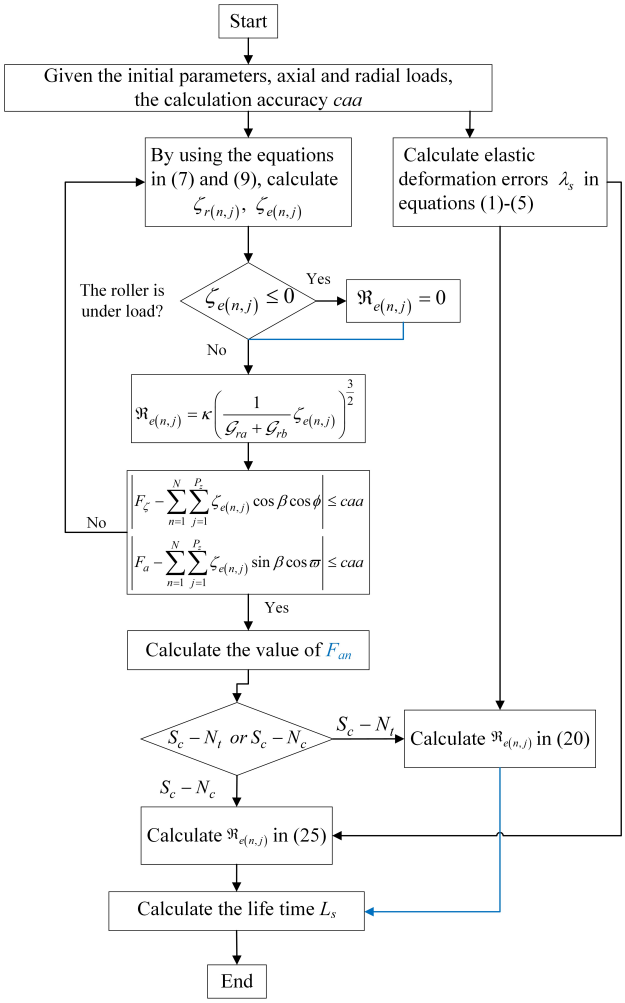

Figure 9. The mechanical behavior analysis flow of the downhole robot system.

Table 2. The designed parameters of the PRSM for the downhole robot system.

Parameters (Unit)	Screw	Roller	Nut
Radius (mm)	15	5	25
Contact angle (°)	45	45	45
Starts	5	1	5
Pitch (mm)	0.8	0.8	0.8
Number	1	10	1
External radius (mm)	/	/	30

Additionally, the left parameters are given as $E = 2.12 \times 10^{11}$ (Pa), $N_0 = 2.5 \times 10^8$, $m_s = 6$.

5.1. The Effects of Axial and Radial Loads

For the downhole robot system, two cases are contained in a complete work procedure. In case 1, the axial loads are chosen to be $F_a = 20$ KN, $F_r = 4$ KN. Additionally, $F_a = 30$ KN, $F_r = 4$ KN in case 2.

From the calculation flow in Figure 9, the corresponding relationship of the contact load and thread number of the two cases can be obtained. The results can be found in Figures 10–15. As depicted in Figures 10–12, the contact load distribution of case 1 for the designed PRSM actuator of the downhole robot system is presented when the PRSM is subjected to axial loads, radial loads, and elastic deformation errors. From Figure 10, the contact loads of all the rollers decreases along the roller axial direction. The results are

consistent with the real application and can be explained as follows. The first several threads bear most of the loads, and the last several threads take only a few loads. Additionally, the #1 and the #10 rollers bear the two largest loads, and the loads that are distributed on other rollers reduce gradually from the radial direction. One can also find that the roller that without radial loads bears the lowest contact load. The result indicates that the radial loads should act on the PRSM as uniformly as possible, which in return can help to design and explore good trajectory planning. It should also be noted that the last two threads of the screw, roller, and nut decrease dramatically for the downhole robot system.

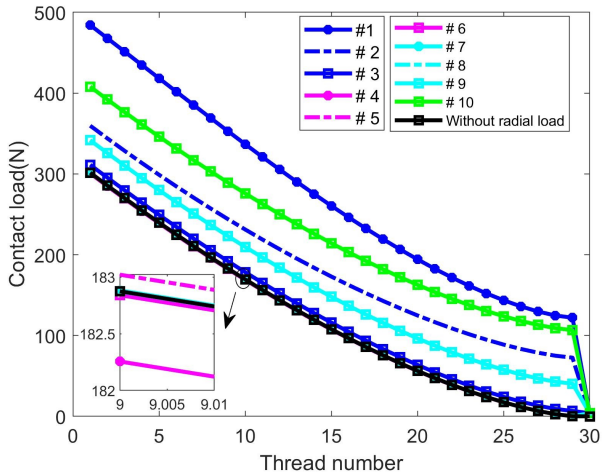

Figure 10. Contact load distribution in different threads of the robot system of case 1.

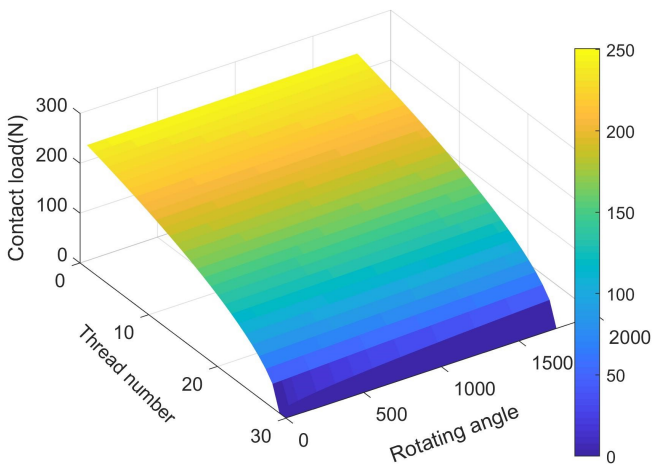

Figure 11. Contact load distribution cycling process without radial load of case 1.

To show the effects of the radical loads on the PRSM, Figures 11 and 12 express the load behaviors in several cycling processes. From Figure 11, we take the first roller as an example. When there are no radial loads, the contact load stays the same in the cycling process, and different threads have their loads. As each roller has the similar load distribution, we only provide the #1 roller of the PRSM. Shown in Figure 12, one can see that the contact load varies when the radial loads are applied to the PRSM. Different from the results in Figure 11, when the radial loads are considered, the bearing force of the roller changes periodically, and different values appear alternately at different positions on the circumference.

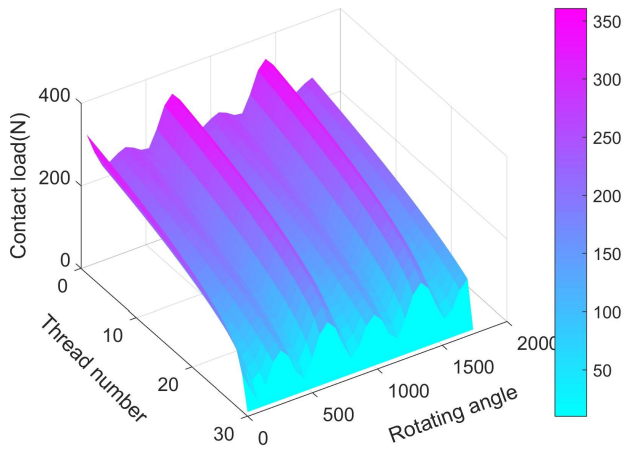

Figure 12. Contact load distribution cycling process with radial load of case 1.

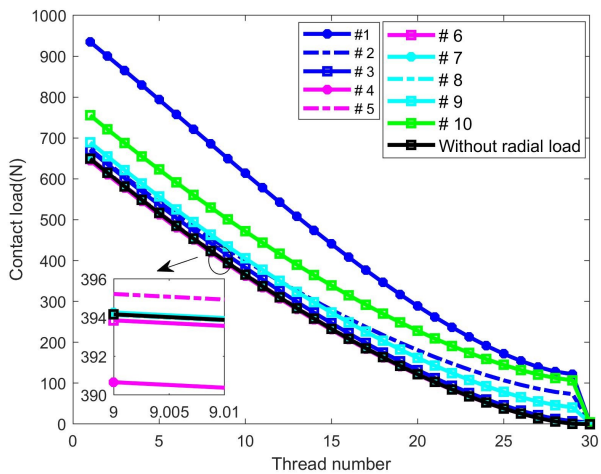

Figure 13. Contact load distribution in different threads of the robot system of case 2.

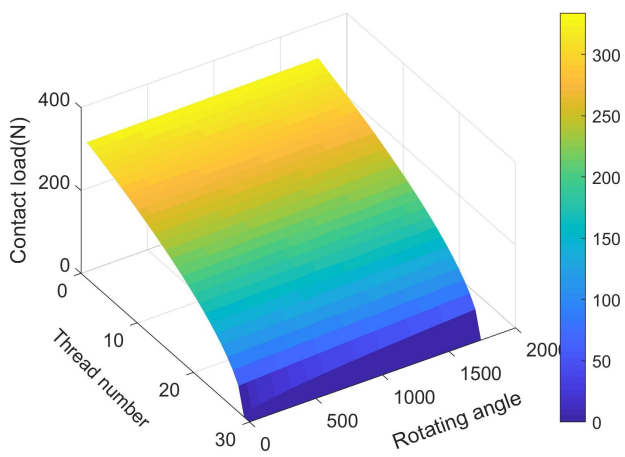

Figure 14. Contact load distribution cycling process without radial load of case 2.

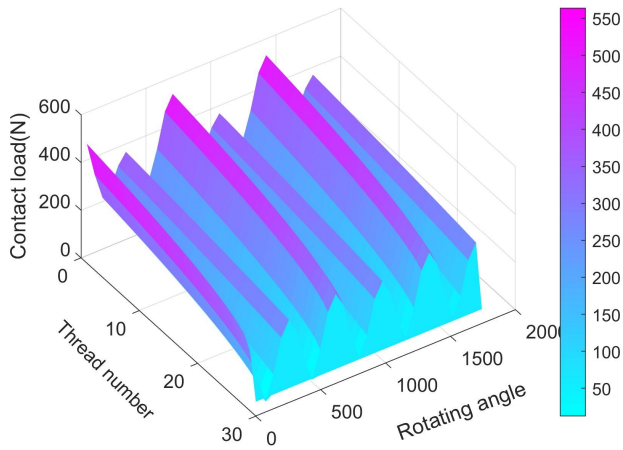

Figure 15. Contact load distribution cycling process with radial load of case 2.

Figures 13–15 show the load distribution behaviors of case 2 for the robot system, where the contact load behaviors are similar to the case 1. For example, the contact load decreases in the axial direction of each roller, and the mechanical behavior of the first and last rollers are the closest but there are still differences. This phenomenon can be understood as follows: on the one hand, the effect of axial loads on the rollers is relatively symmetrical; however, for the robot system, the downhole is not a structural environment, which means that the radial load is not an ideal symmetrical one for the rollers in the circumferential direction. Meanwhile, an angle exists in the first and last roller. As observed from Figures 14 and 15, one can see that the contact load of each thread maintains in the same without radial loads and varies when the external radial loads are applied to the PRSM. As the load distribution behavior of each roller is similar, in this note, we take the first roller as an example. The results show that the radial loads have significant effects on the load distribution, which means that the contact load may be different once the radial loads become inconstant.

5.2. The Effects of Axial Load

Figures 16 and 17 show the load distributions on the threads with different axial loads and the same radial loads. As each roller has a similar load distribution, we take one of them as an example in this note. From Figures 16 and 17, we can see that each load has a corresponding curve. When the PRSM works, the load distribution on the threads will increase on the condition that the axial load increases. On the other hand, the total load reduces along the thread number increasing direction, which has the same tendency in Figures 10 and 13. We can also see from the two figures that the curve has some partial overlap, which means that each thread could be subjected to the same load with the increasing axial load when the PRSM works in both cases of the downhole robot system. The results show us the contact load law of the roller, which gives us the idea that the load optimization could be made based on the results in the two figures, and this part can also extend to our future work.

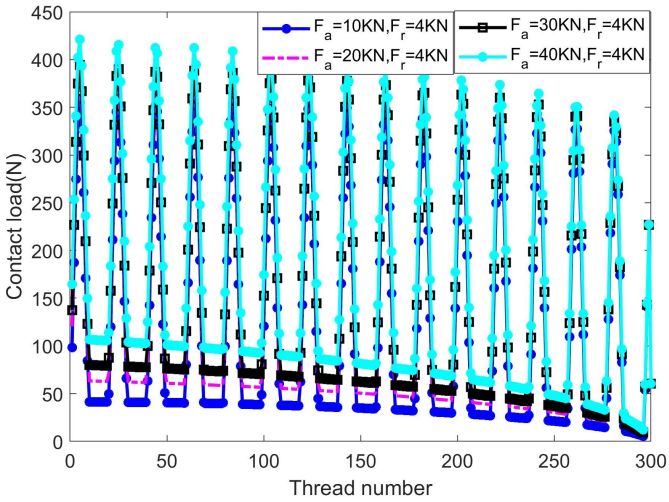

Figure 16. The effects of different axial loads in case 1.

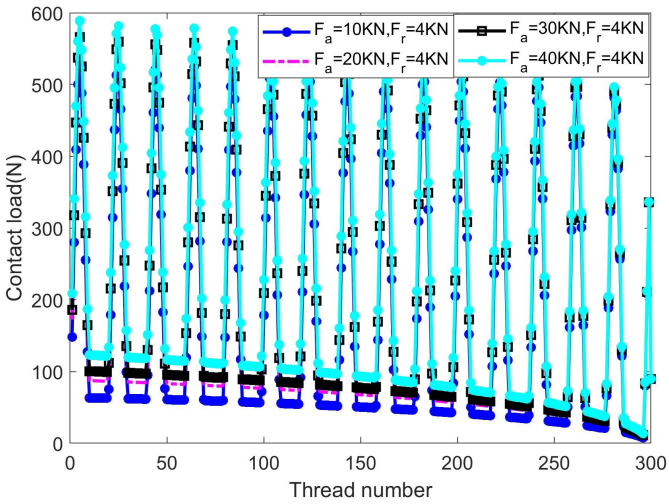

Figure 17. The effects of different axial loads in case 2.

5.3. The Effects of Radial Loads

Figures 18 and 19 express the effects of the radial loads. As depicted before, the downhole is a non-structural environment, and the radial loads are inevitable which have important influences on the PRSM. As expressed in the two figures, when the screw drags the tools to walk forward in the hole or the nut pushes the tools forward, with the growth of the thread number, the load distribution decreases when the PRSM is subjected to a fixed radial load. In Figures 18 and 19, one can see that when there are no radial loads, the total loads are distributed only on the first dozen threads, and the subsequent threads hardly share the loads, which has the same tendency in Figures 10 and 13. From the two figures, we can also see that the total load distribution decreases in the threads' growth direction, and only the radial loads are distributed on the last dozen threads. This means that the radial loads influence each thread, while the axial loads mainly affect the front threads of the PRSM.

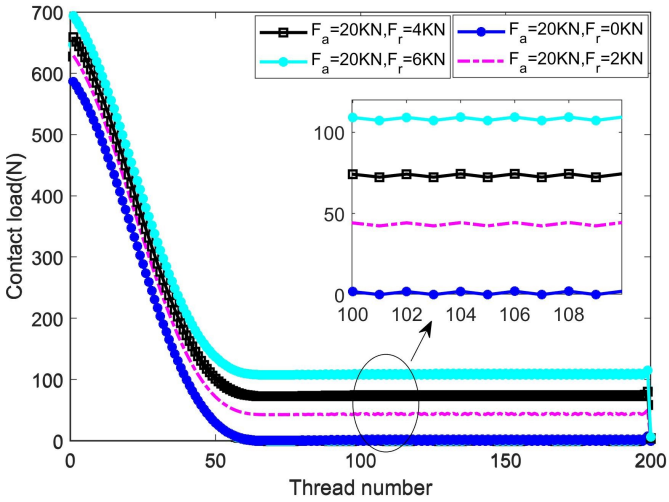

Figure 18. The effects of different radial loads in case 1.

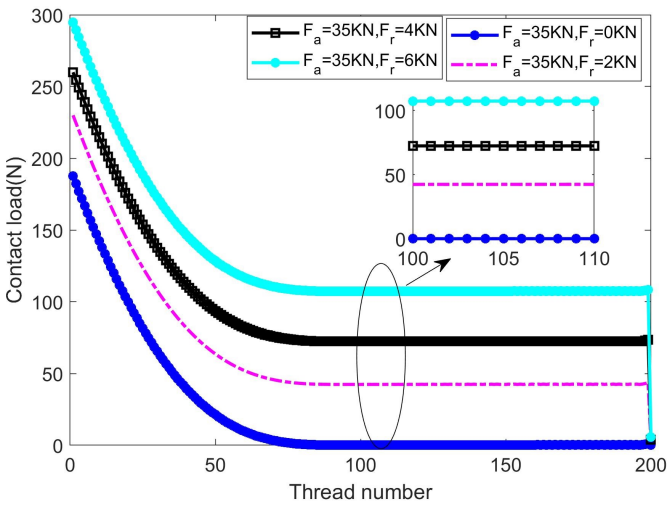

Figure 19. The effects of different radial loads in case 2.

5.4. The Results of the Fatigue Life

Figures 20 and 21 show the results of the fatigue life of the PRSM in case 1, to investigate the effects of external loads on the threads and explore the influences of rotation speeds on the fatigue life. In these cases, we set $w_s = 100$ rpm, $w_s = 300$ rpm, $w_s = 350$ rpm, $w_s = 500$ rpm, and $w_s = 700$ rpm. As shown in Figure 20, we assume that $F_r = 4$ KN, and $F_a = 10$ KN, $F_a = 20$ KN, $F_a = 30$ KN, $F_a = 42$ KN, and $F_a = 55$ KN. We can see from Figure 20 that the fatigue life decreases rapidly first and then decreases slowly with the increase of axial load. More specifically, when the axial loads increase from 10 KN to 20 KN, the fatigue life reduces from nearly 12,000 h to nearly 7000 h. Moreover, when the axial loads increase from 20 KN to 55 KN, the fatigue life reduces from nearly 7000 h to nearly 4000 h, which means that the fatigue life is more sensitive when the axial loads are relatively small and not so sensitive when the axial loads become large. This tendency can also be found in (30). Additionally, from Figure 20, one can also see that the fatigue life reduces sharply with the growth of rotation speed and the same external load. One can also see that the fatigue reduces faster when the axial loads are small and slower when the axial loads become bigger, which implies that the fatigue life is more sensitive under relatively small axial loads and low rotation speed changes.

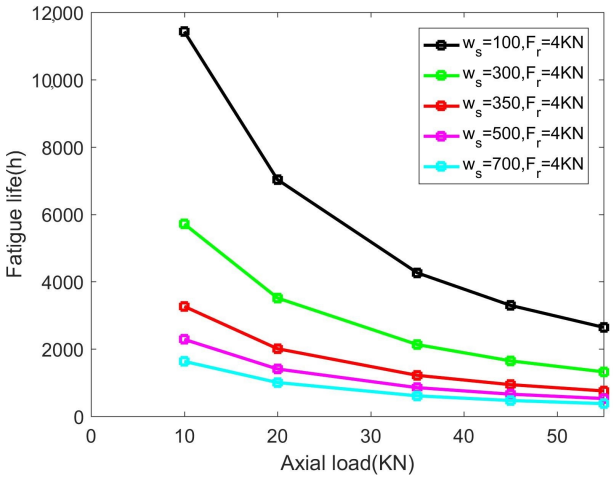

Figure 20. The fatigue life with different axial loads of case 1.

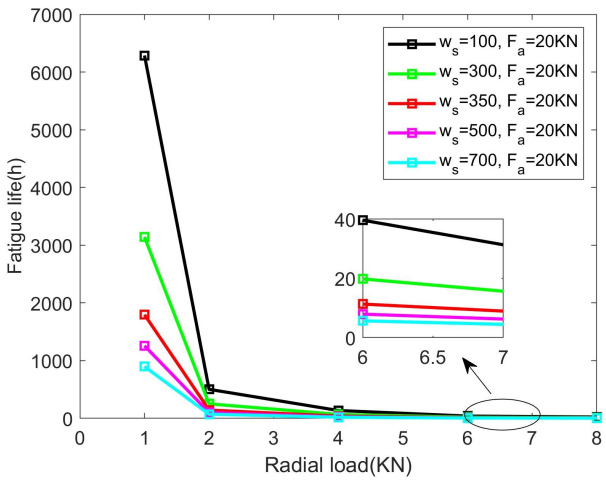

Figure 21. The fatigue life with different radial loads of case 1.

From Figure 21, one can observe that the fatigue life reduces sharply under the condition that the axial loads remain the same while the radial loads increase gradually. More precisely, the fatigue life reduces fast when the radial loads increase from 1 KN to 2 KN, and the fatigue life reduces slower when the radial loads turn 4 KN to 8 KN. Compared with the result in Figure 20, we can see that the fatigue life is more sensitive to the radial loads than the axial loads. Figures 22 and 23 show the results of the fatigue life of the PRSM in case 2. As each roller has a similar tendency, in this subsection, we take one of the rollers as an example. Similar to the results in case 1, the influences of different axial loads, radial loads, and rotation speeds are considered. The results show that the fatigue life reduces sharply at first and then slower, and the variation tendency is similar to case 1. The results in turn indicate that excessive radial force should be avoided as far as possible in the operations of the downhole robot system.

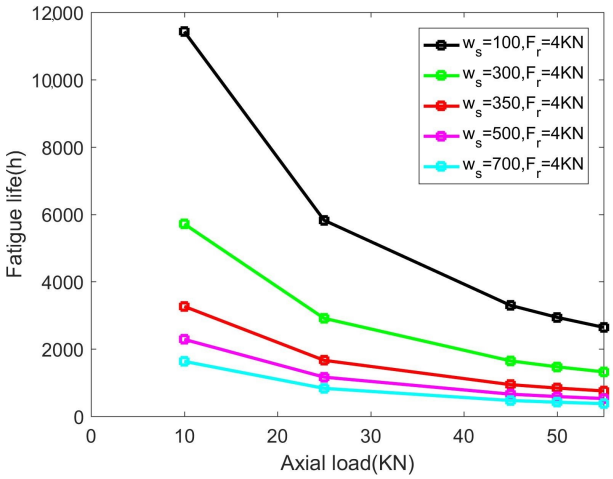

Figure 22. The fatigue life with different axial loads of case 2.

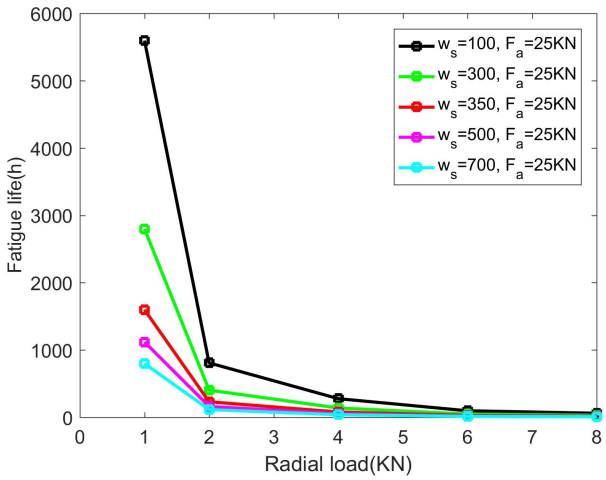

Figure 23. The fatigue life with different radial loads of case 2.

6. Conclusions

In this work, a new downhole robot actuator is presented by introducing the PRSM, and the mechanical behavior analysis is developed for the PRSM during the operations in the downhole environment. The torque and axial elastic deformation errors and the influence of the radial loads are considered when establishing the calculation load distribution model. The fatigue life analysis is also executed. The effects of the axial loads and radial loads on the contact load distribution and the fatigue life are simulated. The following conclusions can be obtained:

(1) The contact load decreases with the thread growth in the downhole robot system when it subjected to radial and axial loads. The first several threads bear most of the loads, and the last several threads take only a few loads. The axial loads are almost distributed on the first several threads while the effects of the radial loads are distributed on each thread.

(2) In the condition that the PRSM works in a different cycling process, when there is no radial load, the contact load stays the same in the cycling process, and different threads have their loads. When the PRSM is subjected to a radial load, the contact load varies periodically, and the mechanical behaviors have similar properties.

(3) For the condition in which the axial loads are different and that in which the axial loads are consistent, the contact load distribution varies and decreases along the axial direction. The tendency in two cases of the downhole robot system stay similar to some degree. Additionally, when the axial loads stay constant and the radial loads

increase, the contact load is distributed only on the first dozen threads while the subsequent threads hardly share the loads.

(4) The rotation speed and external load would affect the fatigue life of the PRSM of the robot system. The fatigue life reduces sharply under the condition that the axial loads, radial loads, and rotation speeds increase gradually. Compared with the axial load, the fatigue life is more sensitive to the radial load, which indicates that the radial load should be as small as possible, and the load distribution optimization could be investigated.

However, the numerical analyses of the stress and strain contours are not simulated in this study, which can help to verify the results of the designed actuator. Indeed, this remains one of the working directions of our study. Additionally, the dynamic analyses, lubrication, and load distribution optimization can also extend to our future work.

Author Contributions: X.D., Conceptualization, methodology, writing—original draft, writing—review and editing; H.Z., Formal analysis, data curation; Q.L., writing—review and editing, investigation, supervision, funding acquisition; Q.W., methodology, review and editing; X.W., formal analysis, resources. All authors have read and agreed to the published version of the manuscript.

Funding: This study was supported by the National Natural Science Foundation of China of FUNDER grant number No. U19A2097.

Institutional Review Board Statement: Not applicable.

Informed Consent Statement: Informed consent was obtained from all subjects involved in the study.

Data Availability Statement: There is no associate data in this study.

Conflicts of Interest: The authors declare no conflict of interest.

Nomenclatures

F_ζ	the radial load
F_a	the axial load
T	driving torque
$\lambda_{a1}, \lambda_{a2}$	the axial deformation caused by the tension load in case 1 and in case 2
λ_b	the axial deformation caused by the driving torque
λ_s	the total deformation error of the screw in the axial direction
ζ_r	the radial deformation
β, ϖ	the contact angle and helix angle
$\mathcal{G}_{ra}, \mathcal{G}_{rb}$	the stiffness coefficients in the contact threads of the screw to roller and roller to nut
$\Im_{S(n,j)}, \Im_{N(n,j)}$	the thread contact loads of the screw and nut
$\hbar_{SZ(n,j)}, \hbar_{ZN(n,j)}$	the contact deformation in the screw to roller interface and the roller to nut with elastic errors
ρ_a	the pitch
E_s, E_N	the elastic modulus of screw and nut
A_s, A_N	the cross sectional areas of screw and nut
$\upsilon_{SZ(n,j-1)}, \upsilon_{SZ(n,j)}$	two consecutive contact surfaces of the screw to roller
$\Re_{SZ(n,j-1)}, \Re_{SZ(n,j)}$	the elastic deformation errors of jth and $(j-1)th$ threads in the screw to roller t interface
$\upsilon_{ZN(n,j-1)}, \upsilon_{ZN(n,j)}$	two consecutive contact surfaces deformations of roller to nut
$\Re_{ZN(n,j-1)}, \Re_{ZN(n,j)}$	the elastic deformation errors of jth and $(j-1)th$ threads in the roller to nut interface
F_{an}	the axial load of the nth roller
N	the numbers of rollers
P_z	the numbers of threads

$\zeta_{sw(n,j)}, \zeta_{st(n,j)}$	the normal contact deformation in the condition without and with the elastic deformation errors
$\lambda_{(n,j)}$	the deformation coefficient
$\varepsilon_{(n,j)}$	the load coefficient
L_S	the fatigue lifetime
w_s	the rotating speed
d_s	the diameter of screw
d_r	the diameter of roller

References

1. Liu, Q.Y.; Zhao, J.G.; Zhu, H.Y.; Wang, G.R.; D.Mclennan, J. Review, classification and structural analysis of downhole robots. *Rob. Auton. Syst.* **2019**, *115*, 104–120. [CrossRef]
2. Zhao, J.G.; Liu, Q.Y.; Zhu, H.Y.; Wang, Z.D.; Liu, W.Q. Nonlinear dynamic model and characterization of coiled tubing drilling system based on drilling robot. *J. Vib. Eng. Technol.* **2019**, *9*, 541–561. [CrossRef]
3. Yue, Q.B.; Liu, J.B.; Zhang, L.G.; Zhang, Q. The posting-buckling analysis and evaluations of limit drilling length for coiled tubing in the sidetrack horizontal well. *J. Pet. Sci. Eng.* **2018**, *164*, 559–570.
4. Abdo, J.; Al-Shabibi, A.; Al-Sharji, H. Effects of tribological properties of water-based drilling fluids on buckling and lock-up length of coiled tubing in drilling operations. *Tribol. Int.* **2015**, *82*, 493–503. [CrossRef]
5. Shang, J.; Fang, d.; Luo,Z.; Wang, R.; Li,X.; Yang,J. Design and analysis of a hydraulic drive downhole traction in-pipe robot based on flexible support structure. *J. Mech. Eng. Sci.* **2021**, *235*, 18–27. [CrossRef]
6. Liu, Q.Y.; Zhao, J.G.; Zhu, H.Y.; Zhang, W. Mechanical model of drilling robot driven by the differential pressure of drilling fluid. *Arab. J. Sci. Eng.* **2019**, *44*, 1447–1458. [CrossRef]
7. Xu, Y.; Wan, Q.F.; Lu, G.; Zhang, B.S. Dynamic characteristics of the end-effector of a drilling robot for aviation. *Int. J. Mater. Sci. Appl.* **2018**, *7*, 192–198. [CrossRef]
8. Duthie, L.; Saeed, A.; Shaheen, S.; Saiood, H.; Moore, B.; Krueger, E. Design transformation of hydraulically powered coiled tubing tractors for matrix acidizing stimulations in extended reach carbonate reservoirs. In Proceedings of the Abu Dhabi International Petroleum Exhibition & Conference, Abu Dhabi, UAE, 13–16 November **2017**.
9. Yao, Q.; Zhang, M.C.; Ma, S.J. Structural design for planetary roller screw mechanism based on the developed contact modelling. *Tribol. Int.* **2022**, *171*, 107570. [CrossRef]
10. Zhou, G.W.; Zhang, Y.H.; Wang, Z.Z.; Pu, W. Analysis of transient mixed elastohydrodynamic lubrication in planetary roller screw mechanism. *Tribol. Int.* **2021**, *163*, 107158. [CrossRef]
11. Yao, Q.; Zhang, M.C.; Liu, Y.S.; Ma, S.J. Multi-objective optimization of planetary roller screw mechanism based on improved mathematical modelling. *Tribol. Int.* **2021**, *161*, 107095. [CrossRef]
12. Fu, X.J.; Liu, G.; Ma, S.J.; Tong, R.T.; C.Lim, T. A comprehensive contact analysis of planetary roller screw mechanism. *J. Mech. Des.* **2017**, *139*, 012302. [CrossRef]
13. Abevi, F.; Daidie, A.; Chaussumier, M. Sartor, M. Static load distribution and axial stiffness in a planetary roller screw mechanism. *J. Mech. Des.* **2016**, *138*, 012301. [CrossRef]
14. Ma, S.J.; Cai, W.; Wu, L.P.; Liu, G.; Peng, C. Modelling of transmission accuracy of a planetary roller screw mechanism considering errors and elastic deformations. *Mech. Mach. Theory* **2019**, *134*, 151–168. [CrossRef]
15. Auregan, G.; Fridrici, V.; Kapsa, P.; Rodrigues, F. Wear behavior of martensitic stainless steel in rolling-sliding contact for planetary roller screw mechanism: Study of the wc/c solution. *Tribol. Online* **2016**, *11*, 209–217.
16. Yao, Q.; Liu, Y.S.; Zhang, M.C.; Liu, G.; Ma, S.J. Investigation on the uncertain factors of the elastic-plastic contact characteristics of the planetary roller screw mechanism. *Proc. Inst. Mech. Eng. Part C J. Mech. Eng. Sci.* **2018**, *233*, 1795–1806. [CrossRef]
17. Ma, S.J.; Wu, L.P.; Fu, X.J.; Li, Y.J.; Liu, G. Modelling of static contact with friction of threaded surfaces in a planetary roller screw mechanism. *Mech. Mach. Theory* **2019**, *139*, 212-–236. [CrossRef]
18. Fu,X.; Li,X.; Ma,S.; Gerada, D.; Liu, G.; Gerada, C. A multi-roller static model of the planetary roller screw mechanism considering load sharing. *Tribol. Int.* **2022**, *173*, 107648. [CrossRef]
19. Zhang, W.; Liu, G.; Ma, S.; Tong, R. Load distribution over threads of planetary roller screw mechanism with pitch deviation. *Proc. IME C J. Mech. Eng. Sci.* **2019**, *233*, 4653–4666. [CrossRef]
20. Mamaev, I.M.; Morozov, V.V.; Fedotov, O.V.; Filimonov, V.N. Harmonic analysis of the kinematic error in a planetary roller screw. *Russ. Eng. Res.* **2016**, *36*, 515–519. [CrossRef]
21. Auregan, G.; Fridrici, V.; Kapsa, P.; Rodrigues, F. Experimental simulation of rolling sliding contact for application to planetary roller screw mechanism. *Wear* **2015**, *332–333*, 1176–1184. [CrossRef]
22. Lepagneul, J.; Tadrist, L.; Sprauel, J.-M.; Linares, J.-M. Fatigue lifespan of a planetary roller-screw mechanism. *Mech. Mach. Theory* **2022**, *172*, 104769. [CrossRef]
23. Du, X.; Chen, B.K.; Zheng, Z.D. Investigation on mechanical behavior of planetary roller screw mechanism with the effects of external loads and machining errors. *Tribol. Int.* **2021**, *154*, 106689. [CrossRef]

24. Jones, M.H.; Velinsky, S.A. Stiffness of the roller screw mechanism by the direct method. *Mech. Based Des. Struct. Mach* **2013**, *42*,17–34. [CrossRef]
25. Zhang, W.; Geng, L.; Tong, R.; Ma, S. Load distribution of planetary roller screw mechanism and its improvement approach. *Proc. Inst. Mech. Eng. Part C J. Mech. Eng. Sci.* **2016**, *230*,3304–3318. [CrossRef]
26. Zhen, N.; An, Q. Analysis of stress and fatigue life of ball screw with considering the dimension errors of balls. *Int. J. Mech. Sci.* **2018**, *137*, 68–76. [CrossRef]
27. Xie, Z.; Xue, Q.; Wu, J.; Gu, L.; Wang, L.; Song, B. Mixed-lubrication analysis of planetary roller screw. *Tribol. Int.* **2019**, *140*, 105883. [CrossRef]